Supporting Information for:

Spin Canting and Slow Magnetic Relaxation in Mononuclear Cobalt(II) Sulfadiazine Ternary Complexes

Cristian Villa-Pérez,*[a] Andoni Zabala-Lekuona,*[b] Iñigo J. Vitorica-Yrezabal,[c] José Manuel Seco,[b] Javier Cepeda,[b] Gustavo Alberto Echeverría[d] and Delia Beatriz Soria*[a]

[a]CEQUINOR (CONICET, CCT – La Plata), Departamento de Química, Facultad de Ciencias Exactas, Universidad Nacional de la Plata, Bv. 120 nº 1465 (1900), La Plata, Argentina.
[b]Departamento de Química Aplicada, Facultad de Química, Universidad del País Vasco/Euskal Herriko Unibertsitatea (UPV/EHU), Paseo Manuel Lardizabal nº3, 20018, Donostia, Spain.
[c]Departamento de Química Inorgánica, Facultad de Ciencias, Universidad de Granada, 18071, Granada, Spain.
[d]IFLP (CONICET, CCT – La Plata), Departamento de Física, Facultad de Ciencias Exactas, Universidad Nacional de la Plata, 47 y 115 (1900), La Plata, Argentina.

Contents:

S1. Crystallographic tables

Table S1.- Crystal data and structure refinement for the complexes.

Complex	**1**	**2**	**3**
Formula	$CoC_{32}H_{26}N_{10}O_4S_2$	$CoC_{28}H_{21}N_6O_2SCl$	$NiC_{28}H_{21}N_6O_2SCl$
Molecular Weight [g mol^{-1}]	737.68	599.96	599.73
Temperature [K]	298(2)	298(2)	232(2)
Wavelength λ [Å]	0.71073 (Mo Kα)	0.71073 (Mo Kα)	0.71073 (Mo Kα)
Crystal system	*P ca*2_1	*P* $2_1/n$	*P* $2_1/n$
Space group	Orthorhombic	Monoclinic	Monoclinic
a [Å]	11.1595(7)	9.2829(6)	9.1866(3)
b [Å]	17.8542(11)	28.894(2)	28.6498(10)
c [Å]	16.0849(8)	10.1698(9)	10.0473(4)
β [º]		99.487(7)	99.955(4)
Volume [$Å^3$]	3204.8(3)	2690.5(4)	2604.58(17)
Z, Density (calculated) [g cm^{-3}]	4, 1.5294	4, 1.4817	4, 1.529
Absorption coefficient μ [mm^{-1}]	0.722	0. 853	0.967
F (000)	1516	1228	1232
θ - range [º]	3.185 - 28.824	2.93 – 26.00	2.177 – 30.009
Index ranges	$-13 \le h \le 12$	$-11 \le h \le 11$	$-11 \le h \le 12$
	$-13 \le k \le 23$	$-35 \le k \le 35$	$-38 \le k \le 38$
	$-20 \le l \le 20$	$-8 \le l \le 12$	$-13 \le l \le 13$
Collected reflections/independent/R_{int}	10260 / 6048 / 0.0403	13041 / 5288 / 0.0763	23391 / 6403 / 0.0535
Completeness to $θ_{máx}$	0.997 (θ = 25.242)	0.998 (θ = 25.242)	1 (θ = 25.242)
Absorption correction		Semi-empirical from equivalents	
Refinement model		Full-matrix least squares on F^2	
Data/Restraints/Parameters	6048 / 7 / 454	5288 / 3 / 358	6403 / 0 / 352
Goodness on fit (F^2)	1.047	1.024	1.057
R_1 indexes [1]	0.0523 (0.0927)	0.0710 (0.1606)	0.0810 (0.0451)
wR_2 indexes (I > 2σ (I)) [2]	0.0884 (0.1054)	0.1236 (0.1576)	0.09654 (0.1068)
Highest peak/hole difference [e $Å^{-3}$]	0.328 / −0.266	0.793 / -0.320	0.368 / -0.423

[1] $R_1 = \Sigma\, ||F_0| - |F_c|| \,/\, \Sigma\, |F_o|$. [2] $wR_2 = [\Sigma w(|F_0|^2 - |F_c|^2)^2 \,/\, \Sigma w(|F_0|^2)^2]^{½}$.

S2. Powder X-ray diffraction analysis

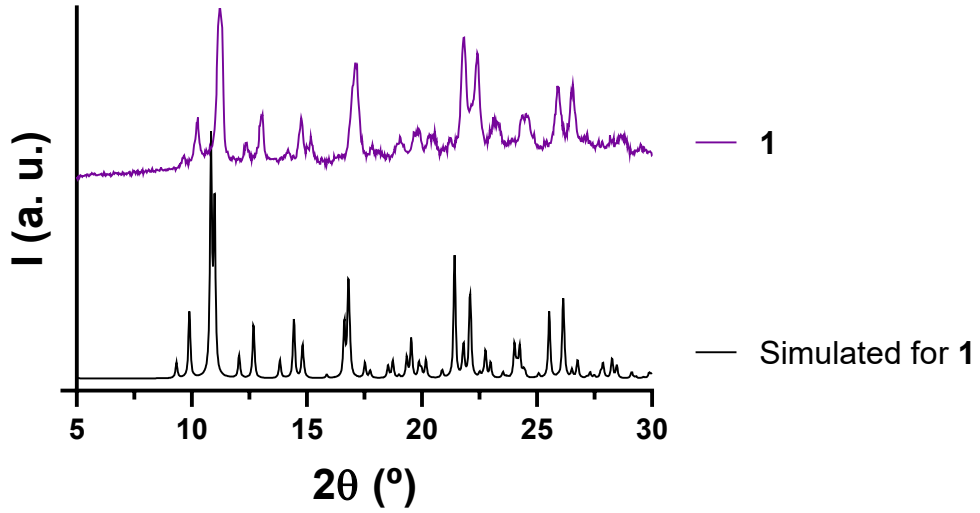

Figure S1.- For compound **1**, simulated pattern from single-crystal X-ray diffraction (black) and experimental XRPD (purple).

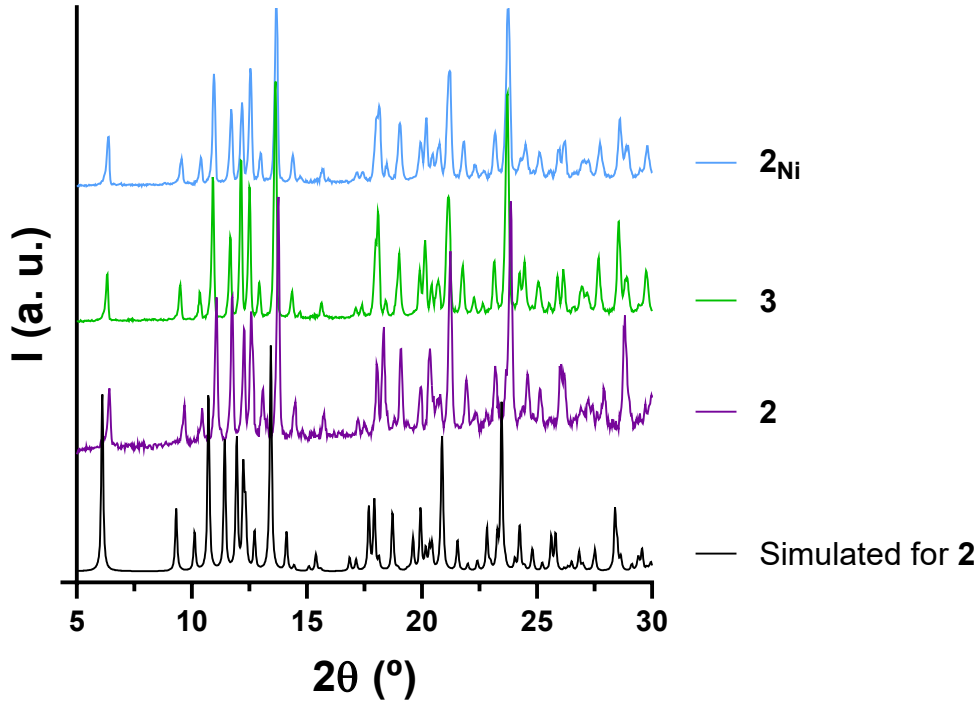

Figure S2.- For compound **2**, **3** and $\mathbf{2_{Ni}}$, simulated pattern from single-crystal X-ray diffraction (black) and experimental XRPD for **2** (purple), **3** (green) and $\mathbf{2_{Ni}}$ (blue).

S3. Continuous Shape Measurements (CShM)

The closer the values to zero, the better-defined geometry

Table S2.- Continuous Shape Measures Calculations for Complex **1**.

HP-6	PPY-6	OC-6	TPR-6	JPPY-6
23.848	23.814	4.464	13.784	27.542

HP-6: Hexagon (D_{6h}); PPY-6: Pentagonal pyramid (C_{5v}); OC-6: Octahedron (O_h); TPR-6: Trigonal prism (D_{3h}); JPPY-6: Johnson pentagonal pyramid - J2 (C_{5v}).

Table S3.- Continuous Shape Measures Calculations for Complex **2**.

PP-5	vOC-5	TBPY-5	SPY-5	JTBPY-5
25.850	4.500	9.133	3.950	10.144

PP-5: Pentagon (D_{5h}); vOC-5: Vacant octahedron (C_{4v}); TBPY-5: Trigonal bipyramid (D_{3h}); SPY-5: Square pyramid (C_{4v}); JTBPY-5: Johnson trigonal bipyramid – J12 (D_{3h}).

S4. Crystal structure: selected bond lengths and angles and additional figures

Table S4.- Selected bond lengths [Å] and angles [º].

Compound 1			
$Co – N_{16}$	2.1934(1)	$N_{16} – Co – N_{31}$	168.08(1)
$Co – N_{17}$	2.1058(1)	$N_{16} – Co – N_{312}$	100.22(1)
$Co – N_{26}$	2.0943(1)	$N_{17} – Co – N_{26}$	96.76(1)
$Co – N_{27}$	2.2761(1)	$N_{17} – Co – N_{27}$	154.62(1)
$Co – N_{31}$	2.1131(1)	$N_{17} – Co – N_{31}$	106.04(1)
$Co – N_{312}$	2.1018(1)	$N_{17} – Co – N_{312}$	102.27(1)
$N_{17} – S_{18}$	1.5977(1)	$N_{26} – Co – N_{27}$	60.88(1)
$N_{27} – S_{28}$	1.6046(1)	$N_{26} – Co – N_{31}$	94.21(1)
		$N_{26} – Co – N_{312}$	160.83(1)
$N_{16} – Co – N_{17}$	62.48(1)	$N_{27} – Co – N_{31}$	88.57(1)
$N_{16} – Co – N_{26}$	90.55(1)	$N_{27} – Co – N_{312}$	100.92(1)
$N_{16} – Co – N_{27}$	103.28(1)	$N_{31} – Co – N_{312}$	78.41(1)
Compound 2			
$Co – Cl_1$	2.2746(2)	$Cl_1 – Co – N_{16}$	99.43(1)
$Co – N_{16}$	2.1166(2)	$Cl_1 – Co – N_{17}$	154.15(1)
$Co – N_{17}$	2.14735(2)	$Cl_1 – Co – N_{21}$	99.40(1)
$Co – N_{21}$	2.0611(2)	$Cl_1 – Co – N_{220}$	107.14(1)
$Co – N_{220}$	2.0393(2)	$N_{16} – Co – N_{17}$	61.87(1)
$N_{17} – S_{18}$	1.6141(1)	$N_{16} – Co – N_{21}$	147.63(1)
		$N_{16} – Co – N_{220}$	119.01(1)
		$N_{17} – Co – N_{21}$	90.98(1)
		$N_{17} – Co – N_{220}$	97.95(1)
		$N_{21} – Co – N_{220}$	79.67(1)
Compound 3			
$Ni – Cl_{03}$	2.2780(7)	$Cl_{03} – Ni – N_{21}$	98.33(6)
$Ni – N_{21}$	1.999(2)	$Cl_{03} – Ni – N_{17}$	155.20(6)
$Ni – N_{17}$	2.101(2)	$Cl_{03} – Ni – N_{22}$	103.35(6)
$Ni – N_{22}$	1.999(2)	$Cl_{03} – Ni – N_{11}$	97.66(6)
$Ni – N_{11}$	2.095(2)	$N_{21} – Ni – N_{17}$	93.92(8)
$N_{17} – S_{18}$	1.617(2)	$N_{21} – Ni – N_{22}$	81.25(9)
		$N_{21} – Ni – N_{11}$	152.67(8)
		$N_{22} – Ni – N_{17}$	99.76(8)
		$N_{11} – Ni – N_{11}$	116.20(9)
		$N_{11} – Ni – N_{17}$	63.63(8)

Table S5.- Intra and Intermolecular Hydrogen bonds in complexes **1**-**3** [Å, º].

D—H···A	**D—H**	**H···A**	**D···A**	**∠ D—H···A**
Compound 1				
N_{117}—H_{117A}···O_{19} [i]	0.85	2.52	3.130(8)	130
N_{117}—H_{117B}···O_{110} [ii]	0.85	2.23	3.054(8)	162
N_{217}—H_{217A}···O_{210} [iii]	0.86	2.55	3.308(10)	147
N_{217}—H_{217B}···O_{29} [iv]	0.86	2.19	3.039(9)	168
C_{112}—H_{112}···O_{110} [v]	0.93	2.58	3.395(7)	147.2
C_{213}—H_{213}···N_{22} [iii]	0.93	2.59	3.490(9)	163.5
Compound 2				
N_{117}—H_{117A}···O_{110} [vi]	0.85	2.25	2.981(7)	143
N_{117}—H_{117B}···Cl_{1} [vii]	0.86	2.53	3.375(6)	168
C_{29} —H_{29}···Cl_{1} [viii]	0.93	2.88	3.641(8)	140
C_{28} —H_{28}···Cl_{1} [ix]	0.93	2.71	3.566(8)	154
Compound 3				
N_{117}—H_{11B}···O_{110} [vi]	0.85	2.15	2.984(3)	160
N_{117}—H_{117B}···Cl_{03} [vii]	0.86	2.51	3.301(3)	150

Symmetry codes: (i) -x, -y+1, z-1/2; (ii) -x+1/2, y, z-1/2; (iii) -x+3/2, y, z-1/2; (iv) -x+1, -y+2, z-1/2; (v) x-1/2, -y+1, z; (vi) x-1/2, -y+1/2, z-1/2; (vii) x-1/2, -y+1/2, z+1/2; (viii) -x, -y, -z; (ix) x-1, y, z.

Table S6.- Structural parameters (Å, º) of π–π interactions of compound **2**.[a]

Ring···Ring[b]	α	DC	β	DZ	Dist.
1A–2A(i)	3.6(3)	3.573(4)	15.8	3.485(3)	3.53–3.69
2A–1A(i)	3.6(3)	3.574(4)	12.7	3.439(3)	3.51–3.63
3A–3A(ii)	0.0(4)	3.696(5)	21.4	3.441(3)	3.45–3.71

[a] Symmetry: (i) —x + 1, –y, –z; (ii) –x + 1, –y, –z + 1. α: dihedral angle between mean planes of the rings (°), DC: distance between ring centroids (Å), β: angle between DC vector and normal to plane(I) (°), DZ: perpendicular distance of the centroids of ring(I) on plane of ring(II) (Å), Dist.: shorter distances between non-hydrogen atoms of rings (I) and (II). [b] Rings: **1A**: N21, C118, C211, C212, C213, C218; **2A**: N22, C23, C28, C29, C119, C210; **3A**: C23, C24, C25, C26, C27, C28.

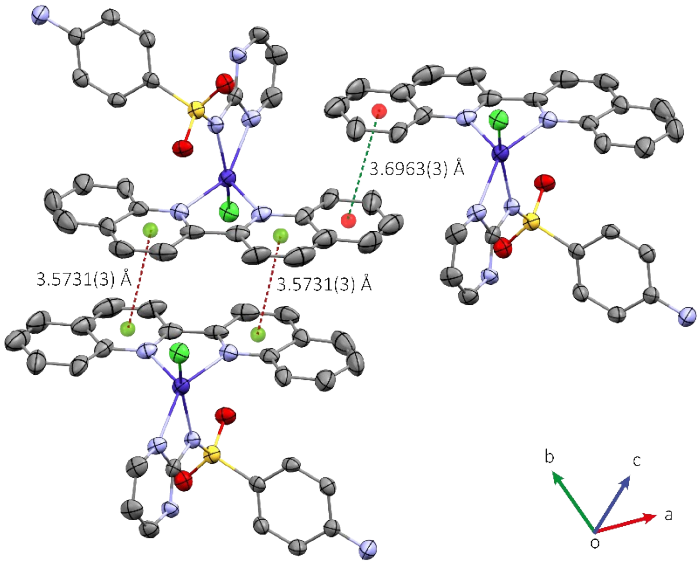

Figure S3.- π-Stacking motifs in complex **2**.

S5. Theoretical calculations

Table S7. NEVPT2 results calculated on the H-optimized structures of compounds **1** and **2** showing the most significant contributions to *D*, *E*/*D*, *g*-tensor and energy-separation between Kramers (KD) doublets.

Compound	**1**	**2**
D (D_{KD1-2}, D_{KD1-3})[a] cm^{-1}	+70.1 (+31.1, +25.4)	–59.4 (–78.5, +14.1)
E/D	0.08	0.21
g_{xx}, g_{yy}, g_{zz}	1.95, 2.52, 2.67	2.03, 2.29, 2.83
g_{iso}	2.38	2.39
ΔE (1-2), ΔE (1-3) cm^{-1}	170, 706	151, 878

[a] The two values in the parentheses after *D* represent the contribution to *D* form the ground to first and ground to second exited state transitions, respectively.

Table S8. NEVPT2 results calculated on the H-optimized structure of compound **3**, showing the most significant contirbutions to *D*, *E*/*D*, and g-tensor.

Compound	**3**
D ($D_{1st\ transition}$, $D_{2nd\ transition}$) cm^{-1}	–21.5 (–60.4, +22.9)
E/D	0.22
g_{xx}, g_{yy}, g_{zz}	2.18, 2.26, 2.37
g_{iso}	2.27

[a] The two values in the parentheses after *D* represent the contribution to *D* form the ground to first and ground to second exited state transitions, respectively.

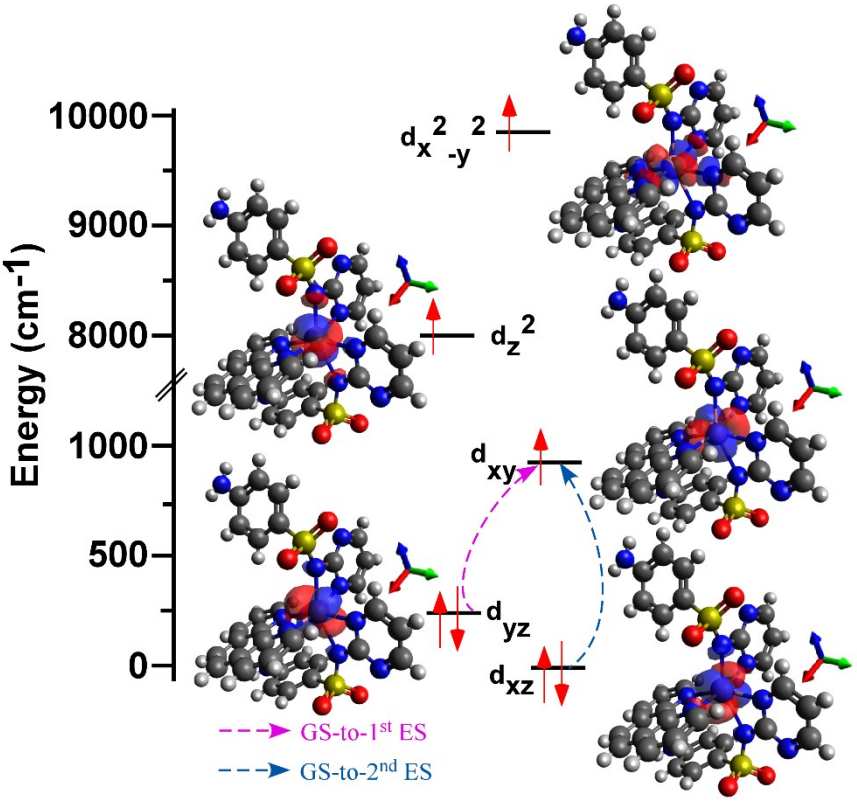

(a)

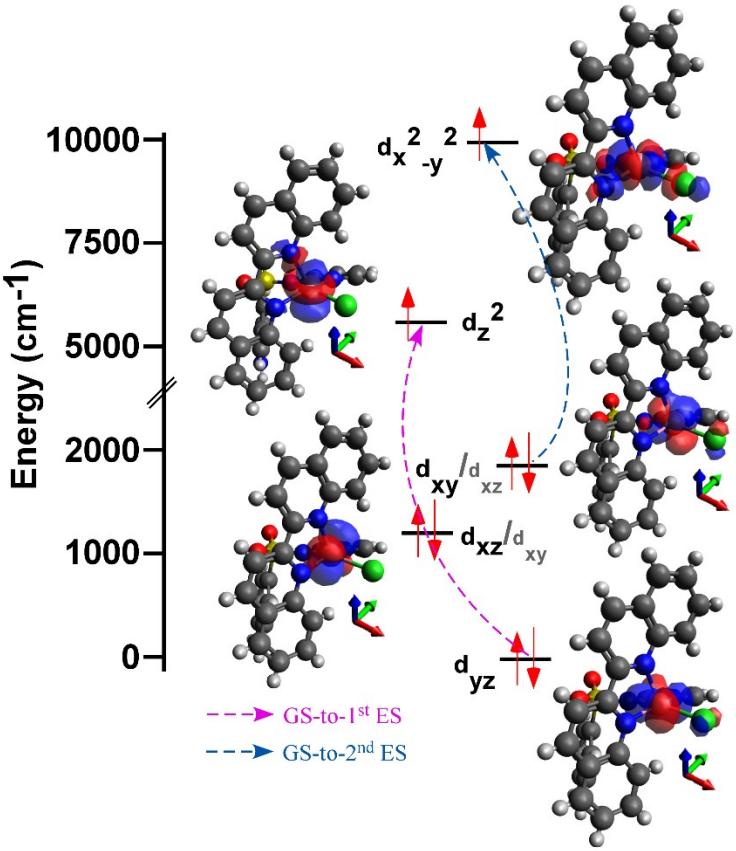

(b)

Figure S4.- NEVPT2-AILFT computed d-orbital splitting for compound **(a) 1** and **(b) 3**. Significant transitions affecting to *zfs* parameters are specified.

Table S9. The ligand field one electron eigenfunctions for compounds **1-3** from NEVPT2.

Compound **1**							
Orbital	**Energy (eV)**	**Energy (cm^{-1})**	**d_{z^2}**	**d_{xz}**	**d_{yz}**	**$d_{x^2-y^2}$**	**d_{xy}**
1	0	0	-0.38656	-0.74310	-0.47033	-0.17081	0.21905
2	0.033	262.9	-0.47011	0.59752	-0.60925	-0.11012	-0.19661
3	0.112	902.4	-0.01538	-0.16647	-0.20768	0.90470	-0.33232
4	0.996	8034.0	0.71319	-0.60305	-0.24404	-0.21512	0.14782
5	1.223	9863.4	-0.24674	-0.10886	0.27239	-0.91387	-0.13386
Compound **2**							
Orbital	**Energy (eV)**	**Energy (cm^{-1})**	**d_{z^2}**	**d_{xz}**	**d_{yz}**	**$d_{x^2-y^2}$**	**d_{xy}**
1	0	0	0.09380	-0.07109	-0.85873	0.37147	0.33278
2	0.156	1256.7	-0.40725	-0.59236	-0.20618	0.10071	-0.65621
3	0.242	1949.2	0.33728	0.59548	-0.29638	-0.06215	-0.66328
4	0.701	5656.1	-0.84002	0.50011	-0.14555	-0.11623	0.09776
5	1.236	9971.6	-0.07718	0.19835	0.33324	0.91351	-0.09566
Compound **3**							
Orbital	**Energy (eV)**	**Energy (cm^{-1})**	**d_{z^2}**	**d_{xz}**	**d_{yz}**	**$d_{x^2-y^2}$**	**d_{xy}**
1	0	0	0.16725	-0.00564	0.94284	-0.16172	-0.23854
2	0.169	1367.0	-0.34389	-0.74721	-0.07256	0.07246	-0.55938
3	0.269	2167.3	-0.19203	-0.51020	0.25466	0.14545	0.78537
4	0.762	6148.3	0.90320	-0.39760	-0.15300	0.05230	0.00247
5	1.46	11773.4	0.03360	0.15251	0.13241	0.97196	-0.11565

Table S10. NEVPT2 computed electronic states and their energies (cm^{-1}), and the corresponding major electronic configurations. Note that minor contributions are not shown.

Compound **1**		
Energy-CASCCF	**Energy-NEVPT2**	**Electronic configurations from CASSCF**
0	0	$d_{xz}^{2}d_{yz}^{2}\,d_{xy}^{1}d_{z^2}^{1}d_{x^2-y^2}^{1}$ (49%) $d_{xz}^{2}d_{yz}^{1}\,d_{xy}^{2}d_{z^2}^{1}d_{x^2-y^2}^{1}$ (25%)
578.7	778.2	$d_{xz}^{2}d_{yz}^{1}\,d_{xy}^{2}d_{z^2}^{1}d_{x^2-y^2}^{1}$ (50%) $d_{xz}^{2}d_{yz}^{2}\,d_{xy}^{1}d_{z^2}^{1}d_{x^2-y^2}^{1}$ (21%)
962.4	1272.2	$d_{xz}^{1}d_{yz}^{2}\,d_{xy}^{2}d_{z^2}^{1}d_{x^2-y^2}^{1}$ (35%) $d_{xz}^{1}d_{yz}^{2}\,d_{xy}^{2}d_{z^2}^{1}d_{x^2-y^2}^{1}$ (16%)
6237.4	8299.1	$d_{xz}^{2}d_{yz}^{1}\,d_{xy}^{1}d_{z^2}^{2}d_{x^2-y^2}^{1}$ (44%) $d_{xz}^{1}d_{yz}^{2}\,d_{xy}^{1}d_{z^2}^{2}d_{x^2-y^2}^{1}$ (26%)
7718.0	8344.3	$d_{xz}^{1}d_{yz}^{2}\,d_{xy}^{1}d_{z^2}^{2}d_{x^2-y^2}^{1}$ (40%) $d_{xz}^{2}d_{yz}^{1}\,d_{xy}^{1}d_{z^2}^{1}d_{x^2-y^2}^{2}$ (21%)
Compound **2**		
Energy-CASCCF	**Energy-NEVPT2**	**Electronic configurations from CASSCF**
0	0	$d_{yz}^{2}d_{xz}^{2}\,d_{xy}^{1}d_{z^2}^{1}d_{x^2-y^2}^{1}$ (47%) $d_{yz}^{2}d_{xz}^{1}\,d_{xy}^{2}d_{z^2}^{1}d_{x^2-y^2}^{1}$ (13%) $d_{yz}^{1}d_{xz}^{2}\,d_{xy}^{1}d_{z^2}^{1}d_{x^2-y^2}^{2}$ (12%)
663.0	908.6	$d_{yz}^{2}d_{xz}^{1}\,d_{xy}^{2}d_{z^2}^{1}d_{x^2-y^2}^{1}$ (41%) $d_{yz}^{1}d_{xz}^{2}\,d_{xy}^{1}d_{z^2}^{1}d_{x^2-y^2}^{2}$ (27%)
1971.9	2649.9	$d_{yz}^{1}d_{xz}^{2}\,d_{xy}^{2}d_{z^2}^{1}d_{x^2-y^2}^{1}$ (59%) $d_{yz}^{1}d_{xz}^{1}\,d_{xy}^{1}d_{z^2}^{2}d_{x^2-y^2}^{2}$ (15%)
4635.3	6215.5	$d_{yz}^{2}d_{xz}^{1}\,d_{xy}^{1}d_{z^2}^{2}d_{x^2-y^2}^{1}$ (49%) $d_{yz}^{1}d_{xz}^{2}\,d_{xy}^{1}d_{z^2}^{2}d_{x^2-y^2}^{1}$ (21%)
6215.2	8314.3	$d_{yz}^{1}d_{xz}^{2}\,d_{xy}^{1}d_{z^2}^{2}d_{x^2-y^2}^{1}$ (51%) $d_{yz}^{1}d_{xz}^{2}\,d_{xy}^{2}d_{z^2}^{1}d_{x^2-y^2}^{1}$ (19%)
Compound **3**		
Energy-CASCCF	**Energy-NEVPT2**	**Electronic configurations from CASSCF**
0	0	$d_{yz}^{2}d_{xz}^{2}\,d_{xy}^{2}d_{z^2}^{1}d_{x^2-y^2}^{1}$ (57%)

		$d_{yz}^{1}d_{xz}^{2}\,d_{xy}^{2}d_{z^2}^{2}d_{x^2-y^2}^{1}$ (24%)
4300.3	6065.6	$d_{yz}^{1}d_{xz}^{2}\,d_{xy}^{2}d_{z^2}^{2}d_{x^2-y^2}^{1}$ (51%) $d_{yz}^{1}d_{xz}^{2}\,d_{xy}^{1}d_{z^2}^{2}d_{x^2-y^2}^{2}$ (19%)
5756.7	8065.6	$d_{yz}^{2}d_{xz}^{2}\,d_{xy}^{1}d_{z^2}^{1}d_{x^2-y^2}^{2}$ (30%) $d_{yz}^{1}d_{xz}^{2}\,d_{xy}^{2}d_{z^2}^{2}d_{x^2-y^2}^{1}$ (28%) $d_{yz}^{2}d_{xz}^{2}\,d_{xy}^{2}d_{z^2}^{1}d_{x^2-y^2}^{1}$ (23%)
7879.9	11371.6	$d_{yz}^{2}d_{xz}^{1}\,d_{xy}^{2}d_{z^2}^{2}d_{x^2-y^2}^{1}$ (50%) $d_{yz}^{1}d_{xz}^{1}\,d_{xy}^{2}d_{z^2}^{2}d_{x^2-y^2}^{2}$ (17%)
9427.0	12753.2	$d_{yz}^{1}d_{xz}^{1}\,d_{xy}^{2}d_{z^2}^{2}d_{x^2-y^2}^{2}$ (45%) $d_{yz}^{2}d_{xz}^{1}\,d_{xy}^{1}d_{z^2}^{2}d_{x^2-y^2}^{2}$ (23%)

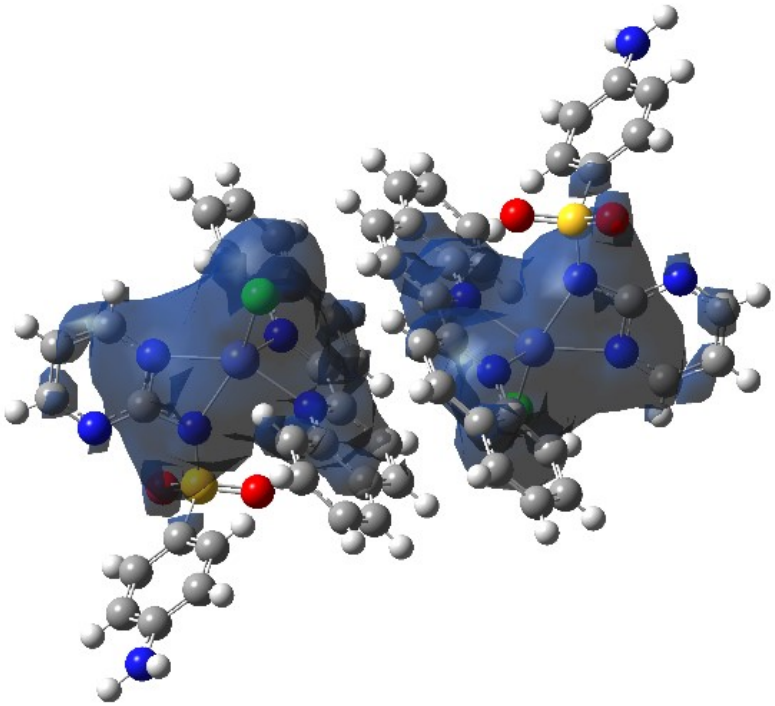

Figure S5.- View of the ground state spin density for compound **2**.

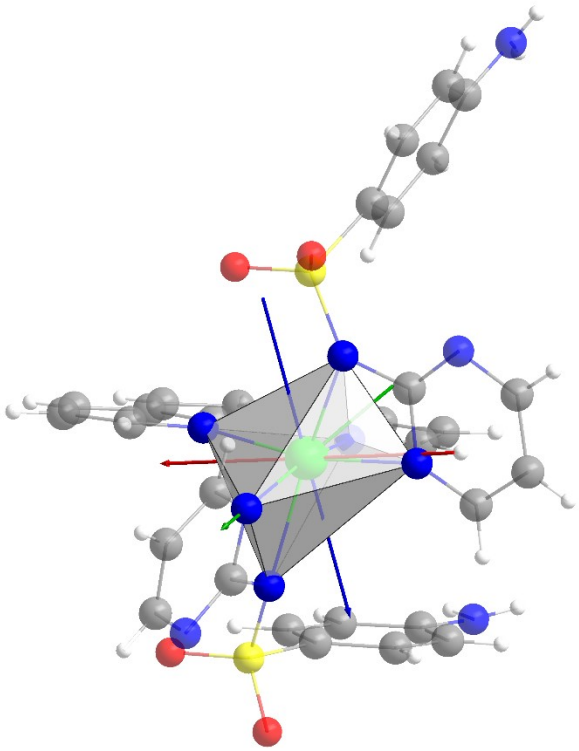

Figure S6.- Orientation of the D-tensor components in Co ion of compound **1** obtained from CASSCF/NEVPT2 calculations. The reference axis x, y and z of the *D*-tensor are displayed in red, green and blue, respectively.

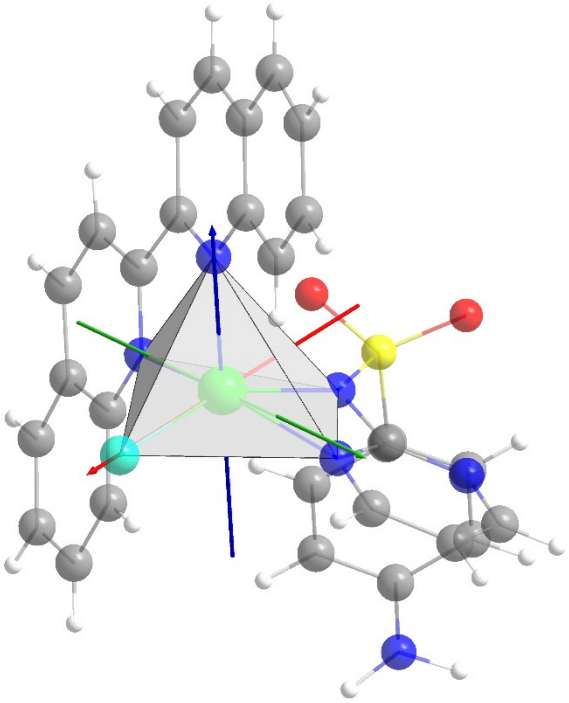

Figure S7.- Orientation of the D-tensor components in Co ion of compound **2** obtained from CASSCF/NEVPT2 calculations. The reference axis x, y and z of the *D*-tensor are displayed in red, green and blue, respectively.

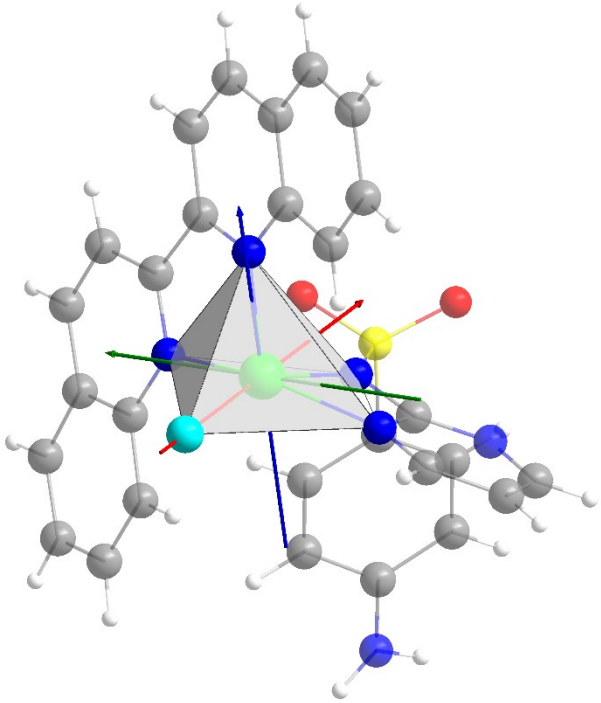

Figure S8.- Orientation of the D-tensor components in Co ion of compound **3** obtained from CASSCF/NEVPT2 calculations. The reference axis x, y and z of the *D*-tensor are displayed in red, green and blue, respectively.

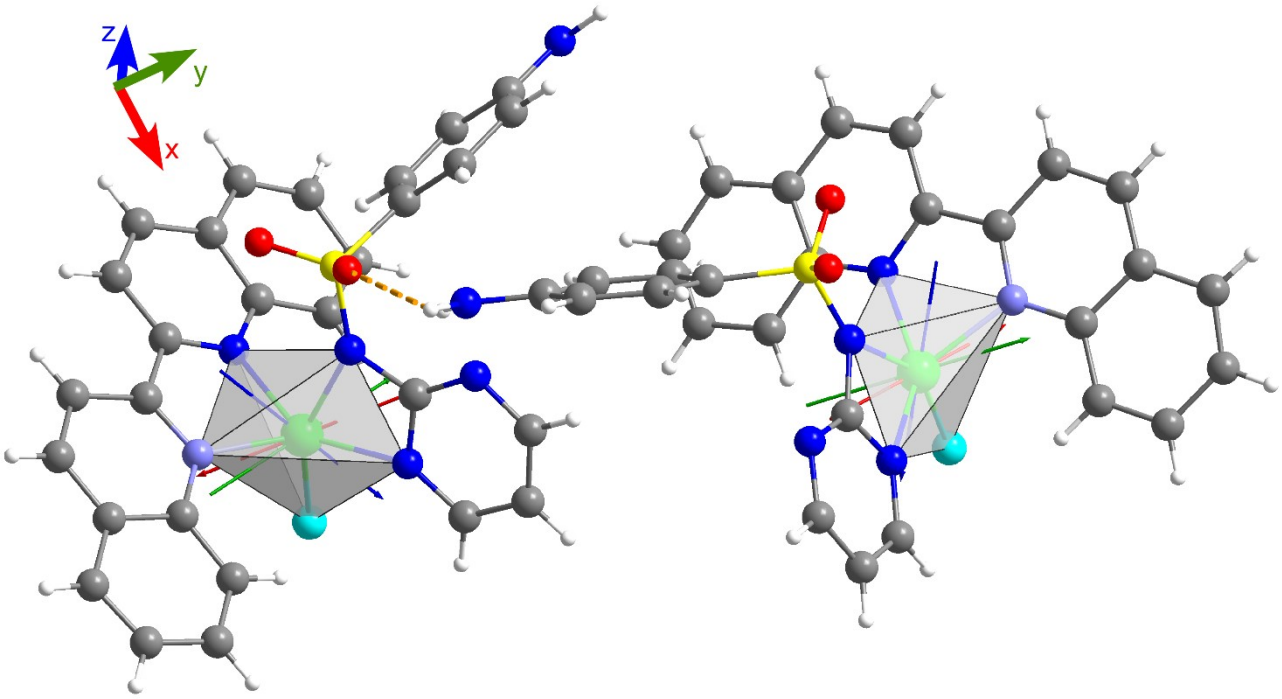

Figure S9.- View of the non-symmetric superexchange magnetic pathway showing the *D*-tensor for both Co centres for compound **2**. Note also that the N atom occupying the apical position of the distorted square pyramid is shown in purple to help visualizing the non-fully antiparallel orientation between both environments.

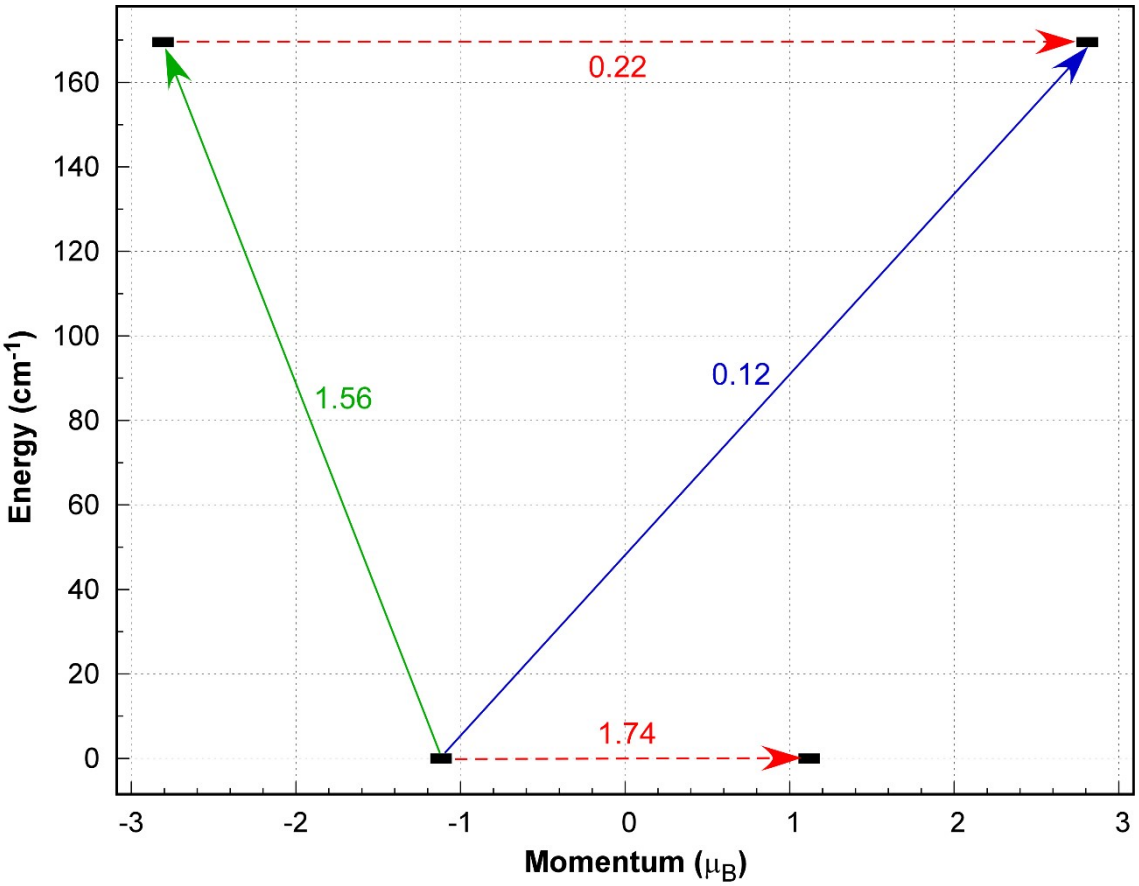

Figure S10.- Ab initio computed relaxation mechanism with the two lowest KDs of compound **1**. Blue and green lines indicate the probable relaxation pathways for magnetization reversal mechanism through excited states. The dotted red lines represents the ground state QTM and TA-QTM (thermally assisted-QTM) via first and second excited KDs. The numbers close to each arrow designate matrix elements of transition magnetic moments.

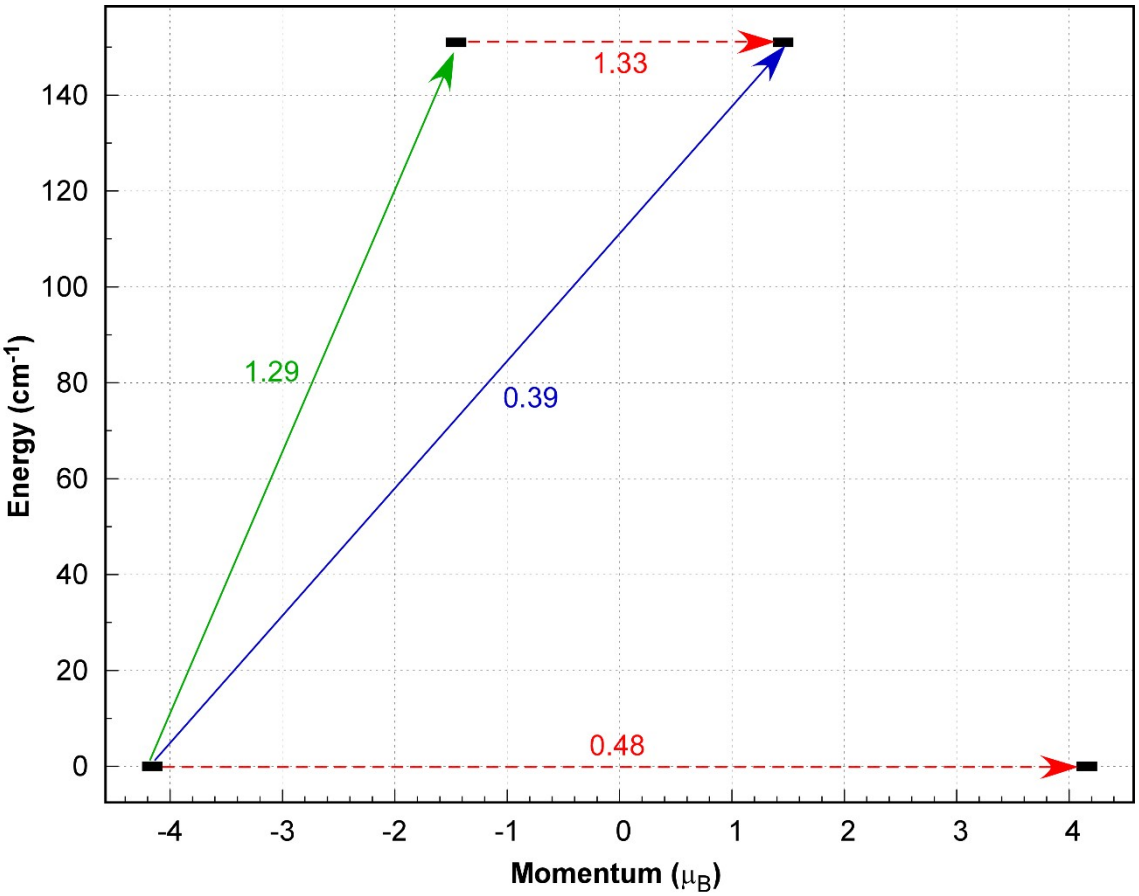

Figure S11.- Ab initio computed relaxation mechanism with the two lowest KDs of compound **2**. Blue and green lines indicate the probable relaxation pathways for magnetization reversal mechanism through excited states. The dotted red lines represents the ground state QTM and TA-QTM (thermally assisted-QTM) via first and second excited KDs. The numbers close to each arrow designate matrix elements of transition magnetic moments.

S6. Static magnetic properties of 3

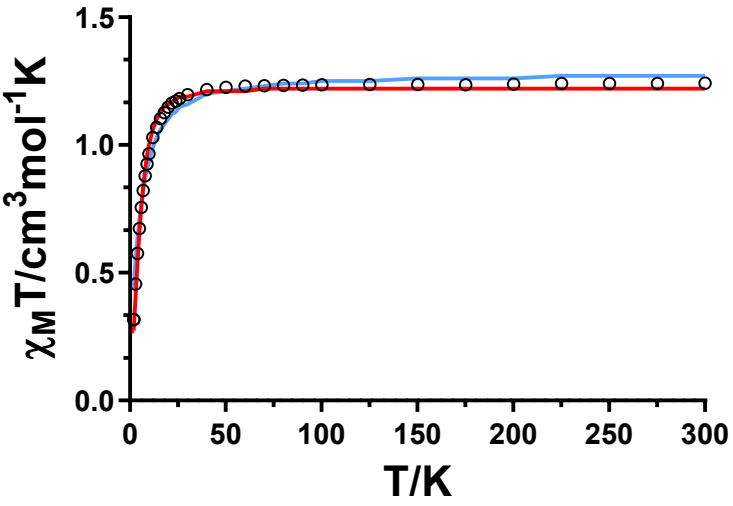

Figure S12.- Variable-temperature dc magnetic susceptibility data for **3** collected under a 1 kOe applied dc field. The red fit was obtained by using the positive *D* value mentioned in the text, while the blue one corresponds to a negative value in addition to antiferromagnetic intermolecular interactions.

S7. Dynamic magnetic properties

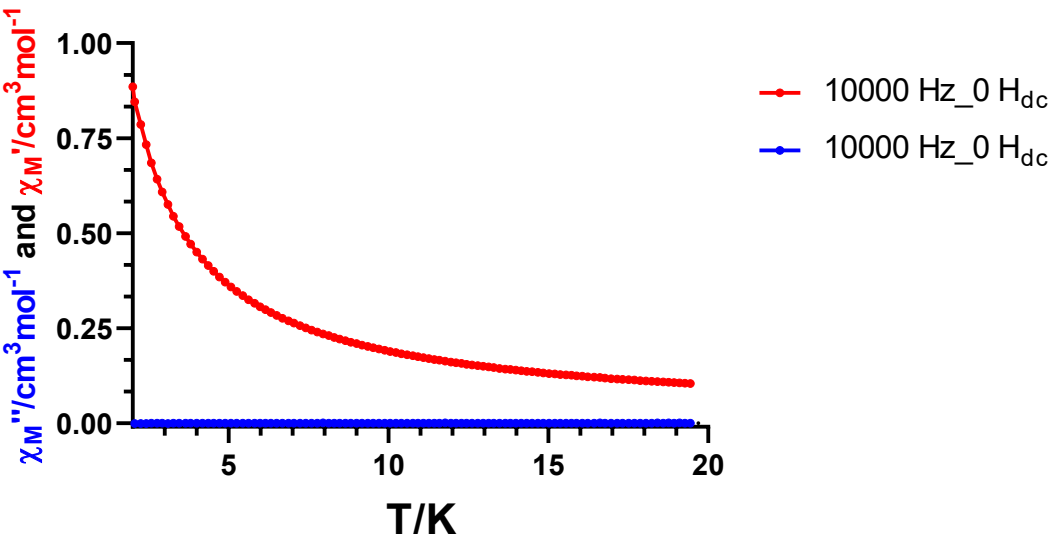

Figure S13.- Temperature dependence of the in phase (red) and out-of-phase (blue) components of the *ac* susceptibility in a zero *dc* applied field for **1**.

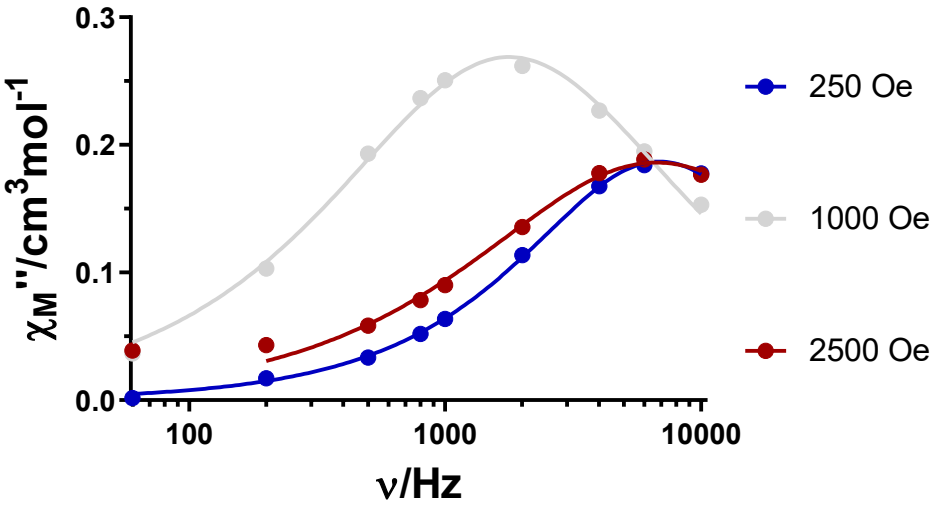

Figure S14.- Field dependence of the out-of-phase signal *vs* frequency at 2.0 K for **1**.

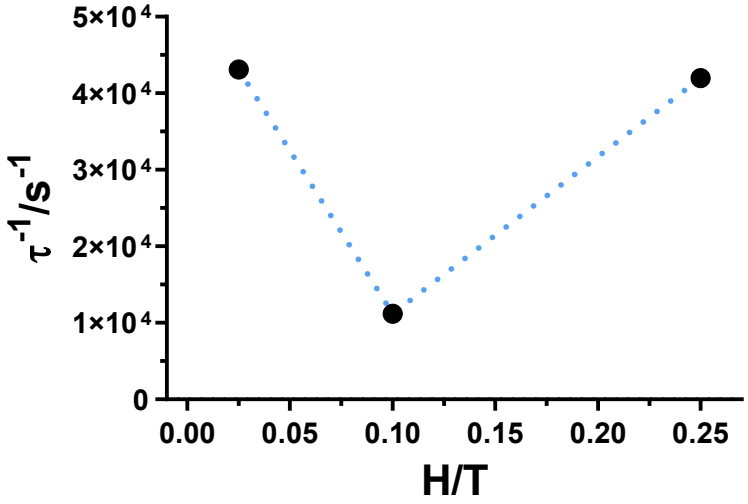

Figure S15.- The inverse of the relaxation times obtained at different magnetic fields at 2.0 K for **1**. The dashed black is a guide to the eye.

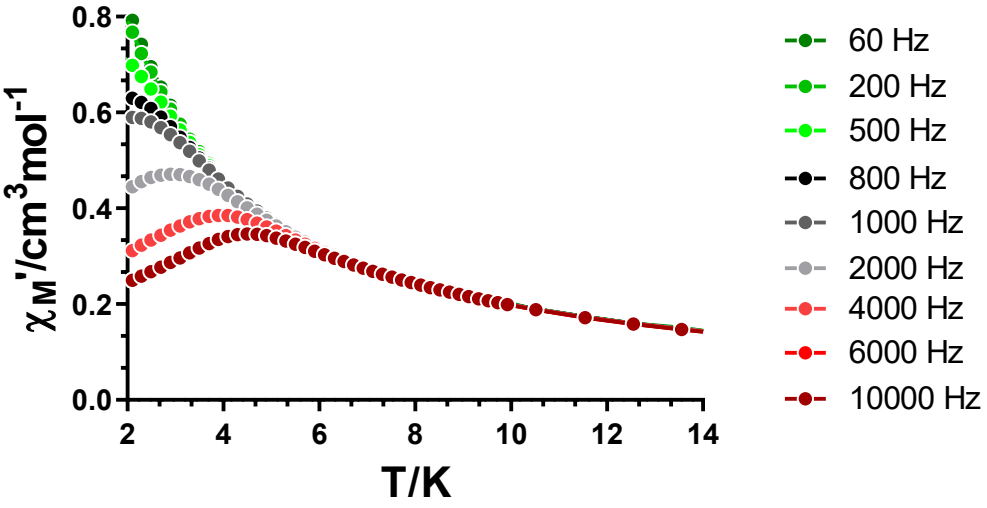

Figure S16.- Temperature dependence of the in phase components of the *ac* susceptibility in a *dc* applied field of 1 kOe for **1**.

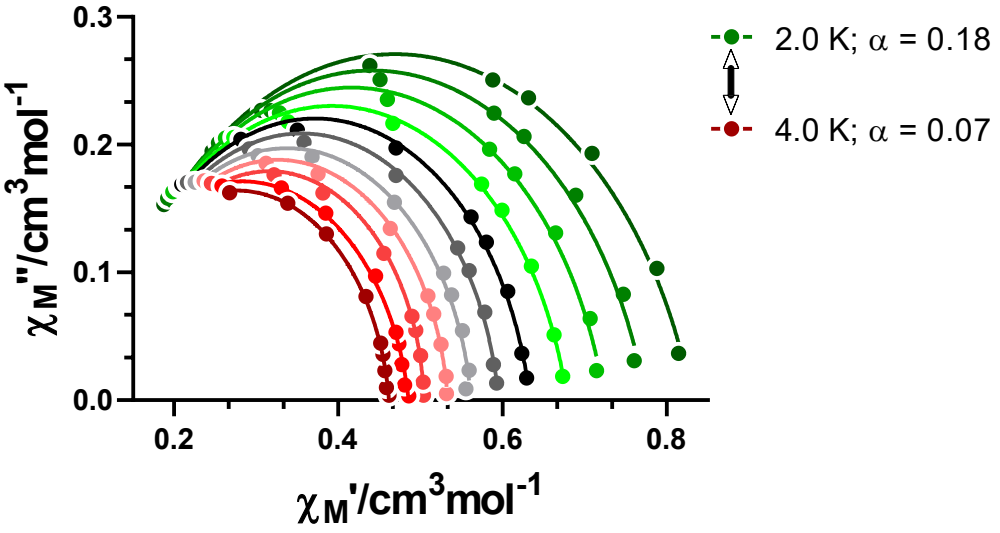

Figure S17.- Cole-Cole plots under 1 kOe field for **1**. Solid lines represent the best fit to the generalized Debye model.

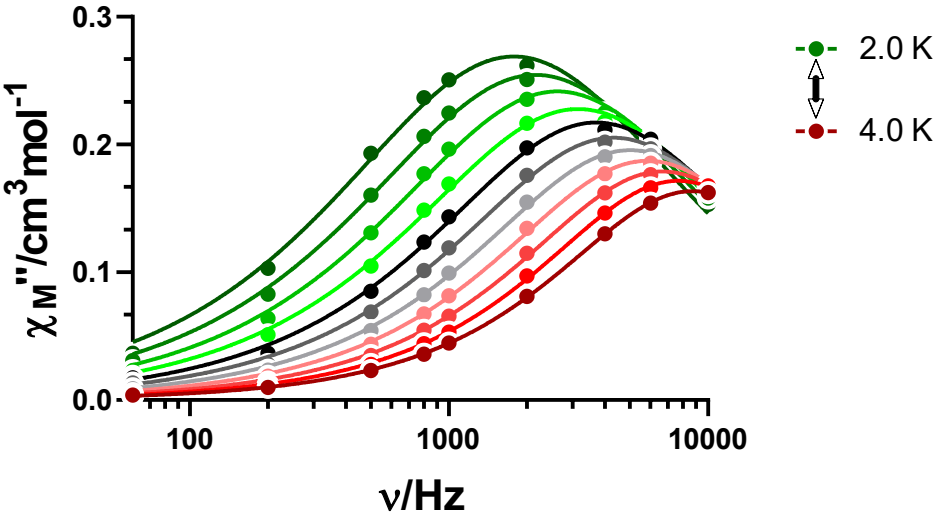

Figure S18.- Variable-temperature frequency dependence of the χ_M'' signal under 1 kOe applied field for **1**. Solid lines represent the best fitting of the experimental data to the Debye model.

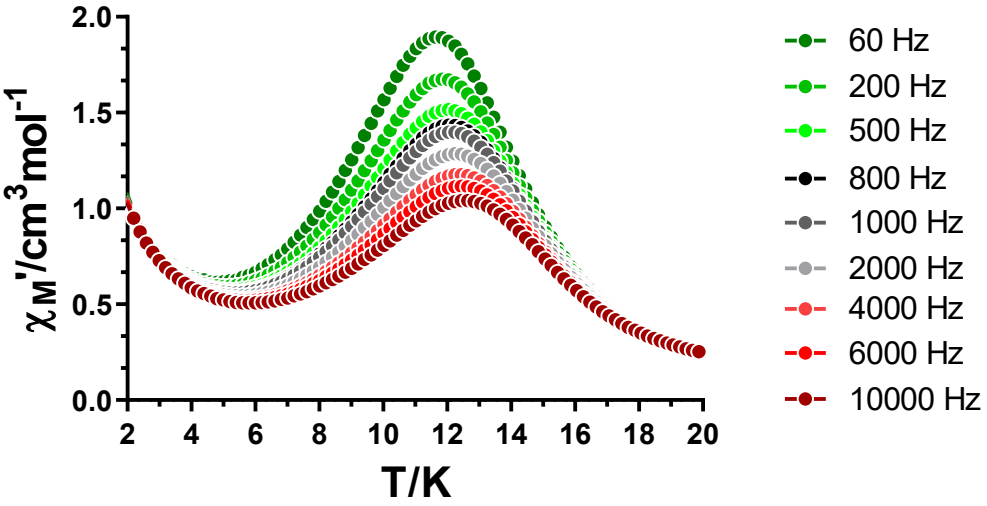

Figure S19.- Temperature dependence of the in phase components of the *ac* susceptibility in a zero applied field for **2**.

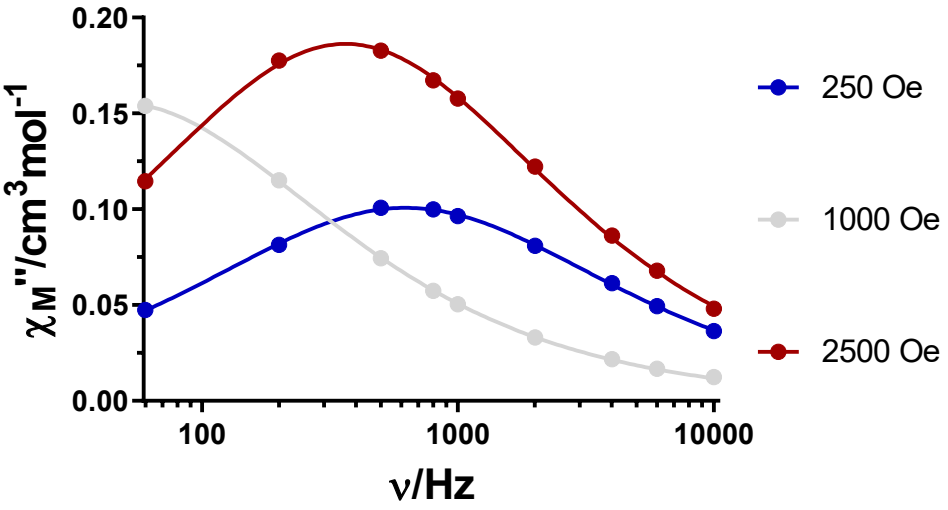

Figure S20.- Field dependence of the out-of-phase signal *vs* frequency at 2.8 K for **2**.

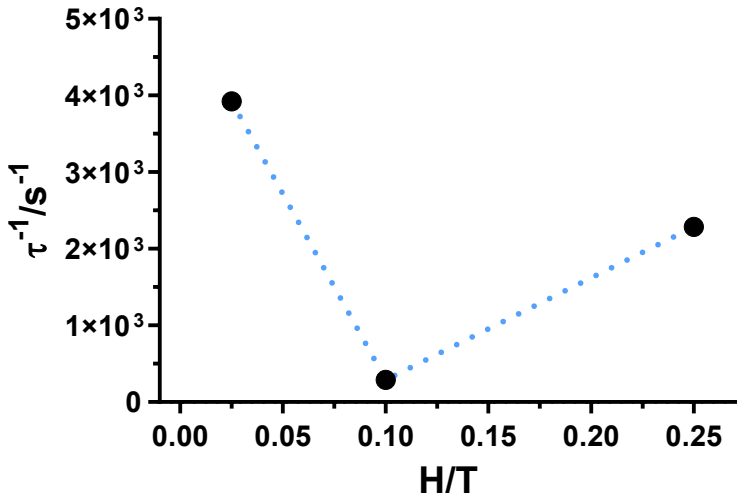

Figure S21.- The inverse of the relaxation times obtained at different magnetic fields at 2.8 K for **2**. The dashed black is a guide to the eye.

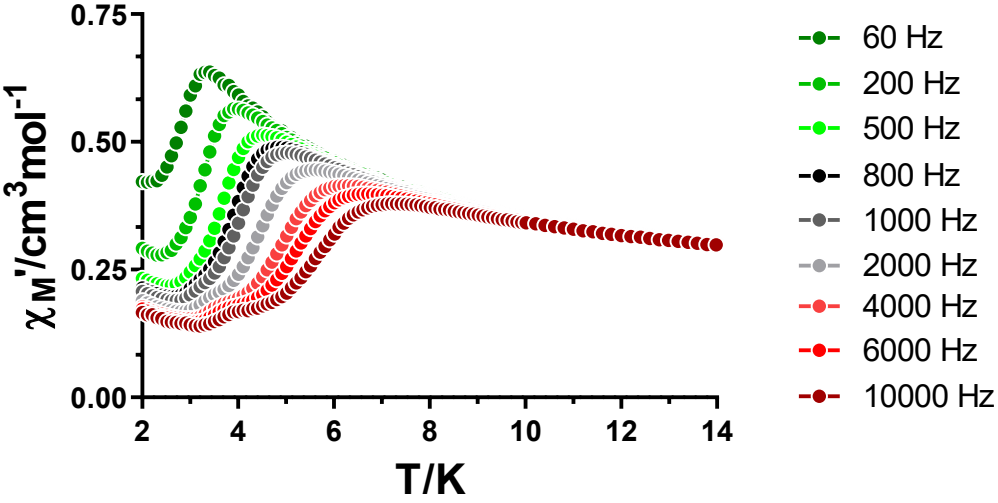

Figure S22.- Temperature dependence of the in phase components of the *ac* susceptibility in a *dc* applied field of 1 kOe for **2**.

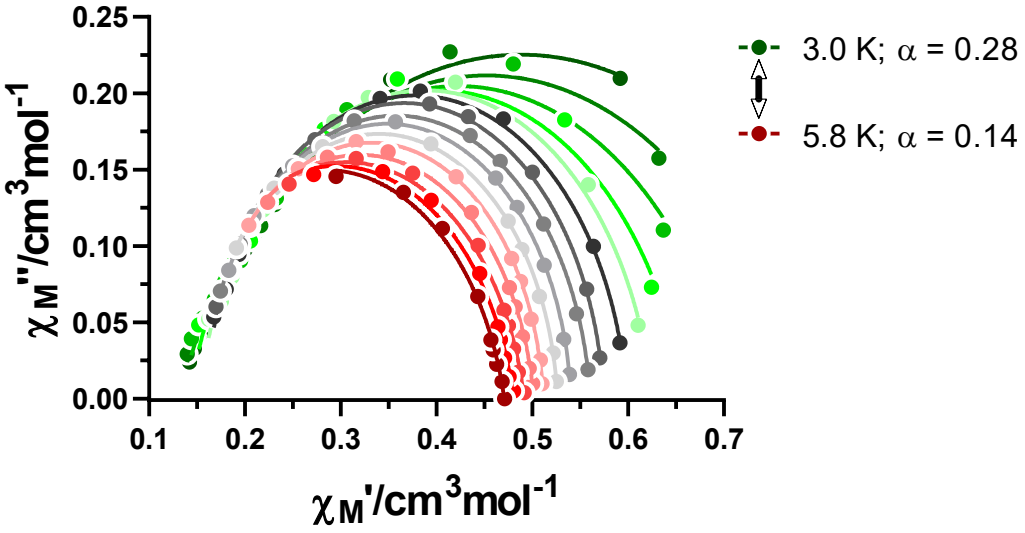

Figure S23.- Cole-Cole plots under 1 kOe field for **2**. Solid lines represent the best fit to the generalized Debye model.

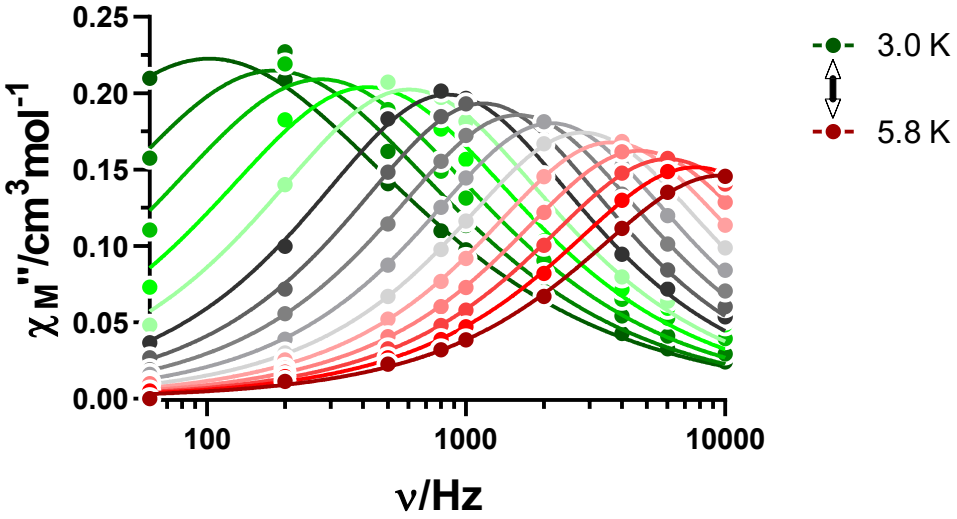

Figure S24.- Variable-temperature frequency dependence of the χ_M'' signal under 1 kOe applied field for **2**. Solid lines represent the best fitting of the experimental data to the Debye model.

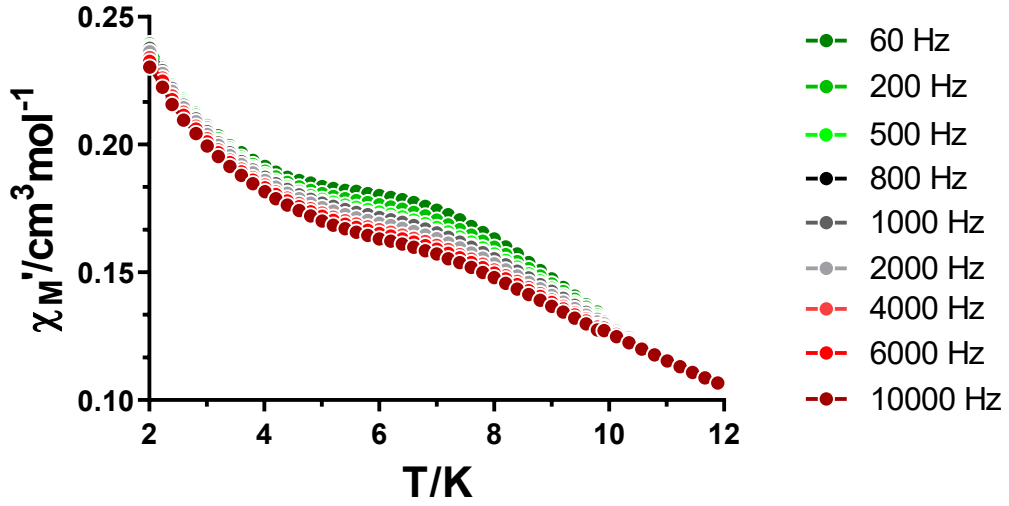

Figure S25.- Temperature dependence of the in phase components of the *ac* susceptibility in a zero applied field for $\mathbf{2}_{Ni}$.

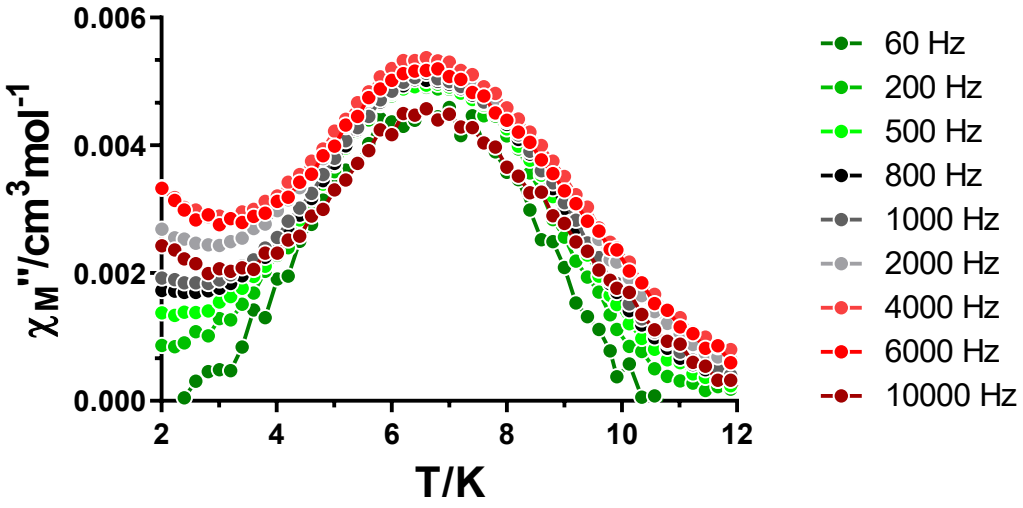

Figure S26.- Temperature dependence of the out of phase components of the *ac* susceptibility in a zero applied field for $\mathbf{2}_{Ni}$.

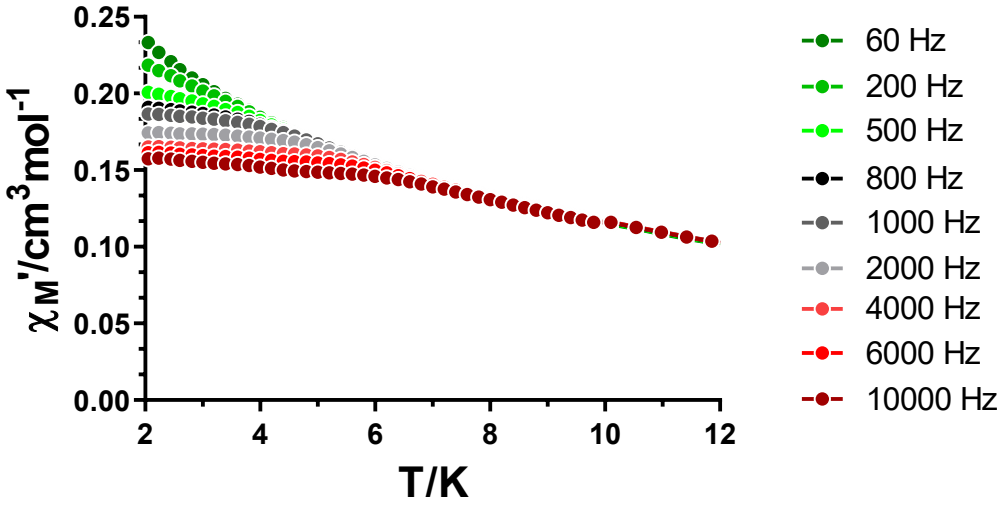

Figure S27.- Temperature dependence of the in phase components of the *ac* susceptibility in a *dc* applied field of 1 kOe for $\mathbf{2_{Ni}}$.

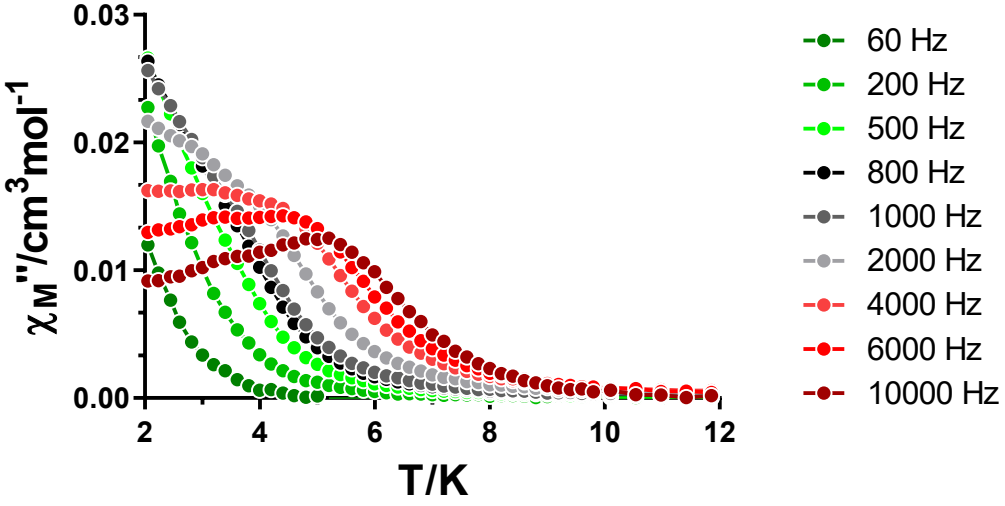

Figure S28.- Temperature dependence of the out of phase components of the *ac* susceptibility in a *dc* applied field of 1 kOe for $\mathbf{2_{Ni}}$.

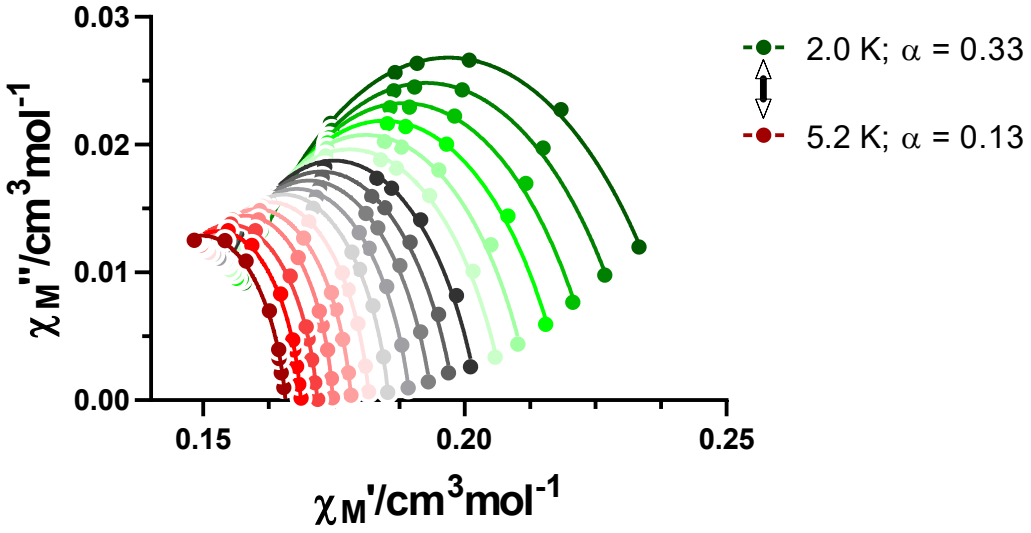

Figure S29.- Cole-Cole plots under 1 kOe field for $\mathbf{2_{Ni}}$. Solid lines represent the best fit to the generalized Debye model.

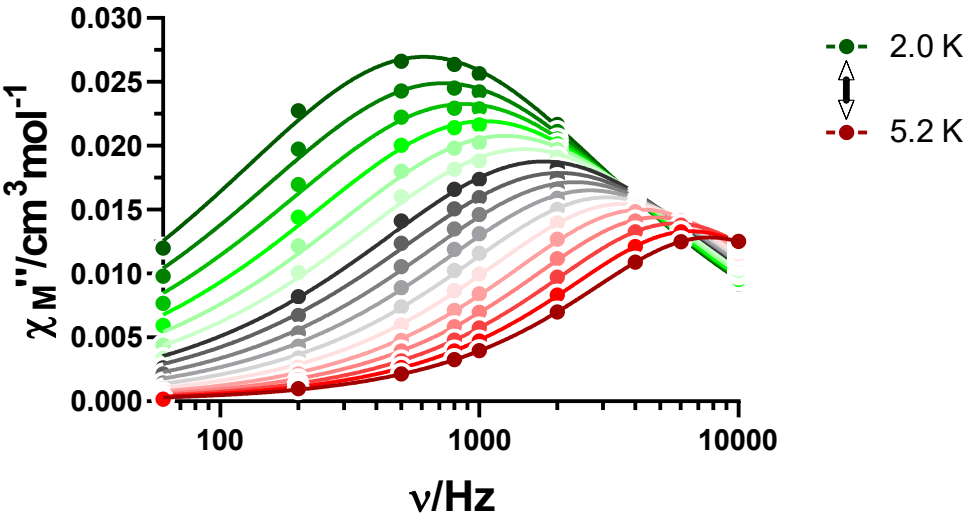

Figure S30.- Variable-temperature frequency dependence of the χ_M'' signal under 1 kOe applied field for $\mathbf{2_{Ni}}$. Solid lines represent the best fitting of the experimental data to the Debye model.

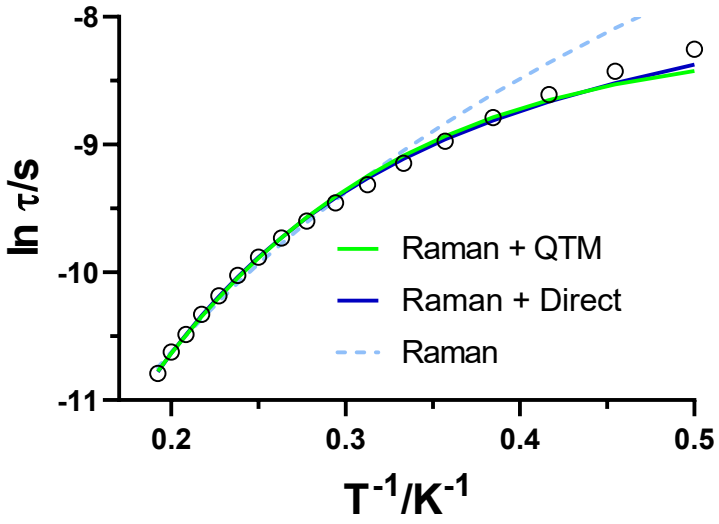

Figure S31.- Alternative fit of the relaxation times for $\mathbf{2_{Ni}}$ considering Raman and QTM mechanisms: B = 83(15) $s^{-1}\cdot K^{-n}$; n = 3.8(1) and τ_{QTM} = 2.9(3)·10^{-4} s ($\tau^{-1} = BT^n + \tau_{QTM}^{-1}$)